Research Article

Abdulkareem Aloraier*, Aniekan E. Ikpe, Husain Aladwani and Esmaeil Almashmoum

Analysis of the combined effects of preheating and welding wire feed rates on the FCAW bead geometric characteristics of 1020 steel using fuzzy logic-based prediction models

https://doi.org/10.1515/jmbm-2025-0067 received March 02, 2025; accepted May 05, 2025

Abstract: Single weld beads were deposited on a steel plate using three different welding wire feed rates (slow, medium, and fast). The samples were preheated before welding at three different temperatures (100, 150, and 200°C). Fuzzy logic models were developed and integrated into the analysis for predicting weld bead geometries. The experimental results demonstrated that preheating and wire feed rates had significant impact on the geometric shape characteristics of 1020 weld beads. Higher preheating temperatures and optimal wire feed rates led to improved weld bead geometry. The integrated fuzzy logic model predicted the weld bead geometry with optimal input variables of 23 V, 150 A, 3 mm/s welding speed, and 540 J/mm heat input, with an optimal bead width, bead height, depth of penetration, heat affected zone (HAZ) width, and height (9.72, 2.02, 1.62, 12.54 and 2.73 mm). The accuracy of the fuzzy models were examined via regression plots, which yielded R^2 values of 0.9146, 0.9909, 0.9467, 0.9805, and 0.8239, for the bead width, bead height, depth of penetration as well as HAZ width and height. This implies that the fuzzy models were effective in predicting the bead height, justifying from its very high degree R^2 value of 0.9909. This showcased the viability of fuzzy logic for predicting weld bead geometry.

Keywords: fuzzy logic, preheating temperature, wire feed rate, bead geometry

Aniekan E. Ikpe: Department of Mechanical Engineering Technology, Akwa Ibom State Polytechnic, Ikot Osurua, Nigeria Husain Aladwani, Esmaeil Almashmoum: Department of Welding, Shuwaikh Industrial Institute, PAAET, Shuwaikh, Kuwait

1 Introduction

Fusion welding is one of the most important processes in the manufacturing industry, with several parameters interacting with one another to determine the performance and quality of welds. The high rate of deposition and effectiveness in joining thick metals have made fluxed cored arc welding (FCAW) a commonly used welding technique in several industries. FCAW applies a tubular electrode integrated with flux during the welding process to protect the weld pool against the effects of atmospheric contaminations. Some welding practices and factors such as the weld bead geometry, preheating temperature as well as the wire feed rate also play a vital role in ascertaining the integrity of a weld. For example, the weld bead geometry, which is characterized by the width, height, and depth of the penetration of a weld, is essential for determining the mechanical properties and structural integrity of a welded joint. On the other hand, the welding wire feed rate is one crucial factor that can influence the bead geometry of FCAW welds, as it directly determines the amount of filler metal deposited into the weld pool. One of the most common welding practices that can influence the weld quality is preheating which to some extent minimizes the risk of cracking, while improving the final quality of the weld. It can aid in improving the cooling rate of the weld metal, which in turn lowers the risk of hydrogen cracking while improving the microstructural integrity of the weld. Studies have shown that heating the base metal before the welding application can lower the induced thermal stress effects, resulting in a more uniform and stable weld. The pulse tungsten inert gas (TIG) welding process parameters of AA 5456 aluminium alloy joint were optimized by Kumar and Sundarrajan [1] using the Taguchi method. Regression models were developed via the analysis of variance (ANOVA) to examine the adequacy of the models that were used to correlate with the observed values. The bead geometry of a joint produced by gas metal arc welding (GMAW) was examined by Thao and Kim [2],

^{*} Corresponding author: Abdulkareem Aloraier, Department of Manufacturing Engineering Technology, College of Technological Studies, PAAET, Shuwaikh, 70654, Kuwait, as.aloraier@paaet. edu.kw

2 — Abdulkareem Aloraier et al. DE GRUYTER

based on actual experimental procedures. The findings suggested that the arc current, welding angle, welding voltage as well as speed had conspicuous effects on the weld bead geometry. Adaptive neuro fuzzy inference system (ANFIS) was adopted by Dhas and Kumanan [3] to predict the welding bead width produced via submerged arc welding (SAW). The experimental process was designed using Taguchi techniques, in which the results obtained were employed for the development of multiple regression models, which trained the intelligent network for accuracy. It was observed that the adopted ANFIS algorithm is flexible and effective for bead width prediction. Kumar [4] adopted the response surface methodology (RSM) regression tool for predicting the relationship between the weld bead geometry and shape produced through the SAW technique. A positive electrode was observed to generate twothirds of the total heat, whereas a negative electrode produced one-third of the total heat. It was further observed that the direct current electrode negative (DCEN) polarity yielded a higher deposition rate and reinforcement compared to the process examined via direct current electrode positive (DCEP) polarity. Gautam and Abbas [5] employed the statistical software Design Expert 8.0, with four [4] factors and five [5] levels, using the central composite design method (CCD) to develop the relationship for predicting weld bead geometry produced by the SAW technique. The RSM algorithm was used for optimizing the process variables while ANOVA was selected for verifying the accuracy of the predicted response, which agreed with the measured values. Balasubramanian et al. [6] applied the clad of AISI 316L on low-carbon steel via FCAW techniques. The FCAW parameters were optimized through RSM while minimizing the weld dilution rate. The optimized input parameters of 14° electrode angle, 0.25 m/min welding speed, voltage of 31 V, 18 mm distance between the nozzle and plate, and wire feed rate of 10 m/min vielded a 6.4% dilution rate with less than 5% error in the predicted percentage of weld dilution. Moreno et al. [7] experimentally determined the geometric characteristics as well as the welding parameters of FCAW techniques for agglutination of SAE 1020 steel flat bars. Maximum width of 11.51 mm, reinforcement of 4.750 mm, penetration of 2.820 mm, penetration area of 13.970 mm², reinforcement area of 33.140 mm², and dilution of 35.188% were obtained at different welding input parameters. Moreno et al. [8] examined the ideal welding parameters and microstructures of welds achieved using the SAE EC410NiMo tubular electrode on SAE 1020 steel material via the FCAW technique. The ideal parameters were a 400 mm/min welding speed and a stick out distance of 33 mm that indicated a convexity index of approximately 30%. Microhardness of the fusion zones was found between 400 and 430 HV_{0.3}, while the EBSD revealed the bainitic area development with a volumetric fraction of martensite stabilization domicile

within HAZ. Abhishek *et al.* [9] employed Utility Taguchi and TOPSIS with the Taguchi S/N ratio to optimize welding parameters *via* metal-cored filler wire for joining ASME SA387 Gr. 11 Cl. 2 steel. The study revealed optimum welding input parameters of 135 A current, 14 V voltage, and 13 L/min gas flow rate. For the output response, the best positive fits included HAZ, depth of penetration, and bead widths of 0.068, 0.159, and 0.087 mm, whereas the worst negative fits determined for the same output response were 0.155, 0.096, and 0.135 mm. The mean response indicated voltage as the most influential input variable.

Tomaz et al. [10] employed an Artificial Neural Network-integrated genetic algorithm for optimizing the input gas tungsten arc welding (GTAW) process parameters of AISI 1020 steel. The ideal predicted welding input parameters were 222 A current, 25 cm/min welding speed, 8 mm nozzle deflection distance, 25° travel angle, and 30 Hz wire feed pulse frequency. These parameters revealed a predicted output response of 6.51 mm bead width, 2.62 mm reinforcement, 0.64 mm penetration, and 15.61 mm dilution, which all correlated significantly with the measured values. The findings further revealed the welding current and speed as the most influential variables on the heat input and melting rate. Colaço and Pintaude [11] considered the Fe-Cr-C hard-facing deposition effect on AISI 1020 steel via flux cored double wire-GTAW technique. The reliability of complete and reduced models developed with RSM was predicted considering the welding current ranging from 185 to 250 A, and welding speed ranging from 10 to 25 cm/min, standoff distance of 10 mm, torch angle of 15°, and wire feed pulse frequency of 60 Hz. For the complete models, a 11.2% width, 25.2% reinforcement, 19.7% penetration, and 3.1% dilution were obtained as relative errors. However, a 8.5% width, 30.8% reinforcement, 15.1% penetration, and 5.7% dilution were obtained as relative errors for the reduced model. The findings further indicated that the welding current and speed are the most influential variables on the weld geometry and dilution. The effects of distinct fluxes on 8 mm-thick grade 304 austenitic stainless steel were investigated by Acharya et al. [12] to examine the weld bead geometry produced by the TIG method. A 3-factor 3-level RSM with the Box-Behnken design method and experimental sequence of 15 runs were employed. A ternary flux mixture comprising SiO2, TiO2, and Fe2O3 of various proportions (72:18:10, 65:25:10, and 45:45:10) was applied. An optimum penetration depth of 6.507 mm, bead width of 8.58 mm as well as reinforcement value of 0.0 were obtained from the welding parameters of 160 A current, 1.778 kJ/mm heat input, flux ratio of SiO₂/TiO₂/Fe₂O₃ of 65:25:10, and root gap as 1.4 mm.

Linear and nonlinear models were employed by Yang et al. [13] to compare the fatigue crack expansion rate on

welds of a steel storage. The results revealed that the nonlinear model is more reliable in predicting the expansion rate. Fuzzy reliability analysis (FRA) of corroded pipelines was adopted by Bagheri et al. [14] to assess the model reliability index from multiple fuzzy-random variables (FRVs). From the findings, FRVs had significant effects on the corrosion defect, depth, and operating pressure in terms of fuzzy reliability index (FRI). The sensitivity level of the FRA indicated that the FRI of the corroded pipelines of X100 high-strength steel is more sensitive compared to the FRVs. Based on the nature of uncertainty, the wiper structural system was modelled by Liang et al. [15], using interval method, universal grey number theory, and enumeration approach. The findings revealed that the universal grey number theory is a reliable approach that can adequately analyse uncertain structural systems, including weld geometry. However, adaptive surrogate-model-based reliability evaluation method can yield optimal balance between predictive efficiency and accuracy [16-18], making it a promising approach in the domain of reliability assessment of weld bead geometric characteristics. Multiple fatigue models were considered from linear and nonlinear cumulative fatigue damage (NCFD) models by Liu and Ma [19] to conduct data analyses, aiming at fatigue life for metals. The findings revealed that the NCFD is an adequate representation of fatigue damage under constant and multistage variable amplitude loading. Therefore, considering the complex uncertainty of the model within the domain of the fatigue damage, and integration of advanced machine learning strategies to minimize the forecasting error was suggested.

Several studies have been carried out on the effects of welding parameters and materials such as the low carbon steels in welding. For instance, AISI 1020 steel considered in this study is a low carbon steel grade with a wide range of structural applications due to its excellent weldability and machinability. Understanding how these parameters influence the weld quality is necessary for optimizing the welding process and ensuring the structural integrity of the welds. This study investigated the effects of preheating and the welding wire feed rate on the bead geometry of 1020 steel using the FCAW process. The objective was to analyse the combined effects of preheating and welding wire feed rates on the FCAW bead geometric characteristics of 1020 steel with integrated fuzzy logic algorithm (FLA) for prediction of weld bead geometry. The novelty behind the adoption of fuzzy logic-based computational tools in this study is its robust framework, which adequately demystify the inherent uncertainties and complexities associated with FCAW processes. Traditional predictive models oftentimes rely on deterministic approaches that may fail to capture the nuanced interactions between multiple variables, such as preheating temperature and wire feed rates.

However, fuzzy logic-based models accommodate the vagueness and imprecision that characterize real-world welding scenarios. By employing linguistic variables and membership functions, these models offer a simplified and intuitive approach for representing the relationships between input parameters and output characteristics, such as the bead width, height, and penetration depth.

2 Materials and methods

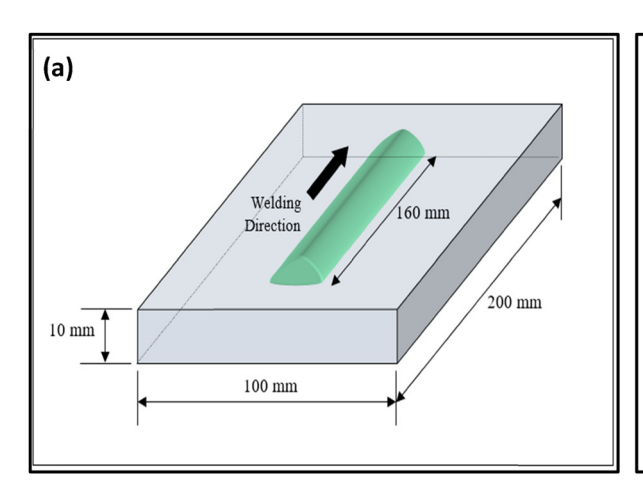
The materials and methods utilized while analysing the combined effects of preheating and welding wire feed rates on FCAW geometric bead characteristics of 1020 steel with integrated FLA for prediction of weld bead geometry are presented and discussed under this section.

2.1 Materials

Materials employed in conducting the experimental procedures of this study included AISI 1020 carbon steel, acetone, FCAW machine, welding gun, CO₂ shielding gas, welding electrode, precision cutting machine, epoxy resins, fine grit abrasive papers, Nital etchant, and metallurgical microscope.

2.2 Methods

Twelve samples of AISI 1020 carbon steel were cut into 200 mm × 100 mm × 10 mm, as shown in Figure 1(a). Surfaces of the cut samples were thoroughly cleaned with acetone to remove accumulated oxides. The bead on plate experiments was carried out and the dimensions and location of the bead are shown in Figure 1(b). The ESAB FCAW machine was utilized, as shown in Figure 2. The shielding gas was CO₂ to allow deep penetration. Each of the samples prior to welding were properly positioned in the welding fixture. The FCAW welding parameters, including the voltage, current, welding speed, and heat input, were adjusted in the machine, and the samples were welded ensuring adequate travel speed and torch angle. The samples were prepared for micrographs. All samples were transversely cut using precision cutting machine to measure the bead geometry, including the bead width and height, depth of penetration, and the heat affected zone (HAZ) width and height. The cut sections of each sample were mounted in epoxy resins to retain microstructural integrity during



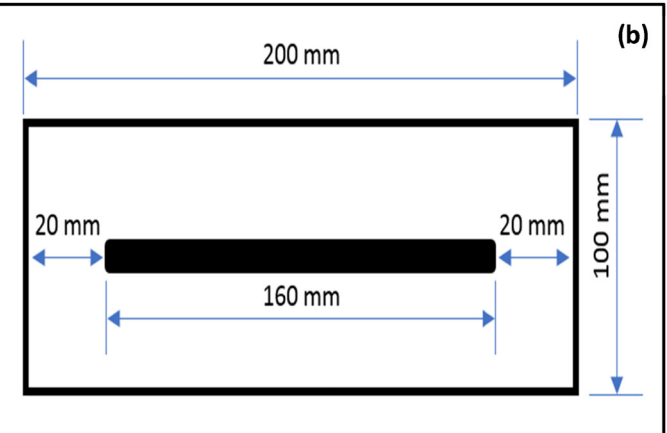


Figure 1: (a) Presentation of the plate sample dimensions and (b) top view of weld bead location.

polishing. The samples were ground via progressively finer grit abrasive papers to remove undesired surface coatings, polished with alumina suspension and etched with Nital etchant. The etched samples were examined through a metallurgical microscope at different magnifications, and high-resolution images of the fusion zone, HAZ, and base metal were captured. The bead geometry of the weld regions is presented in Figure 3(a), while different areas of the weld region are illustrated in Figure 3(b). The sectioned coupon of the post-weld sample is presented in Figure 4. Table 1 shows the chemical composition and the mechanical properties of AISI 1020 carbon steel samples used. FCAW is a complex process that involves numerous variables, including but not limited to thermal fluctuations, material inconsistencies, and operator variability. As a result, three experimental trials were replicated per welding condition to mitigate the effects of random variability inherent in the experimental processes. This was done to provide room for accurate estimation of the mean and variance of the bead

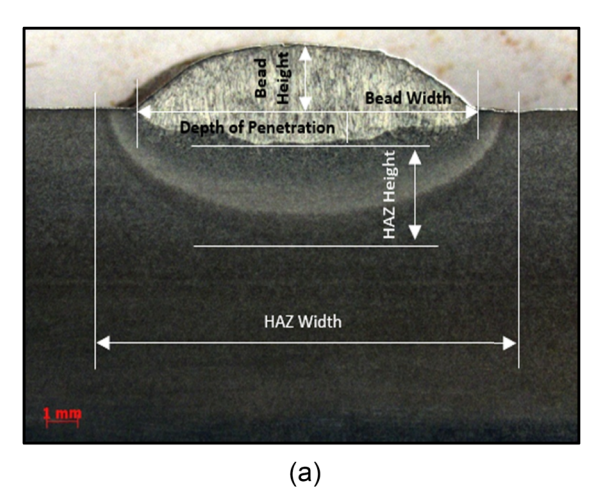
geometric characteristics, thus providing a clearer picture of the underlying trends and effects attributable to the independent variables of preheating and wire feed rates.

2.2.1 Process parameters used in the experimental procedure

The parameters employed in the experimental process included a gas flow rate of 20 L/min; slow, medium, and fast wire feed rates of 2.5, 5, and 10 m/min, respectively; CO_2 shielding gas; AWS E71T-1C electrode type; 1.2 mm welding wire diameter (electrode size); $200 \times 100 \times 10$ mm³ plate dimensions; DC + welding current and polarity; and 80% process efficiency. The sample notations are presented in Table 2, and the input welding parameters are shown in Table 3. H_1 , H_2 , and H_3 represent different temperatures where the samples were preheated prior to welding operation, and H_0 signifies the ambient



Figure 2: FCAW welding machine used in the experiment.



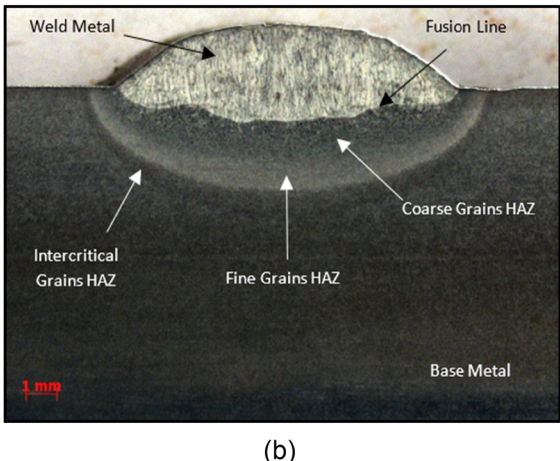


Figure 3: (a) Locations of measurements (bead geometry and HAZ). (b) Cross section of the bead on a plate showing different areas of the weld.



Figure 4: Coupon sampling (transversely).

temperature of the samples prior to preheating. To ensure optimal performance of the 1020 steel during welding applications, correct ambient temperatures of the samples were essentially maintained between 21 and 32°C before heating. This temperature range allowed the steel to retain

its mechanical properties, while preventing unwanted welding defects. Similarly, S_1 , S_2 , and S_3 represent slow, medium, and fast wire feed rates.

2.2.2 Fuzzy logic modelling

The fuzzy logic modelling process was initiated by the selection of linguistic input variables, conversion of input variables to fuzzy sets, generating the membership functions profiles, applying rule-based commands, and converting output response to non-fuzzy values (defuzzification). These profiles are illustrated in Figure 5(a) and (b).

The three membership functions selected as each input parameter for the prediction of weld bead geometric output variable were low, moderate, and high. Applying FLA in modelling the weld bead geometry of AISI 1020 low carbon steel achieved *via* the FCAW process is a complex procedure that commenced with identifying the input parameters and their ranges that influenced the output responses [20]. This was achieved by determining the key parameters that influence the geometric characteristics of FCAW beads, which included low

Table 1: Chemical composition and mechanical properties of AISI 1020 steel

Chemical composition	С	Si	Mn	Р	S	Cr	Sn	Cu	Ni
	0.196	0.2	0.577	0.013	0.007	0.043	0.049	0.07	0.012
Mechanical properties	Tensile (ultima	e strength ate)	Tensile s (yield)	trength	Young's modulus	Bulk modulus	Poisso- n's ratio	Elongation at break	Brinell hardness
	390-46	50 MPa	240-380	MPa	200 GPa	140 GPa	0.29	15-30%	110-130

Table 2: Sample notations

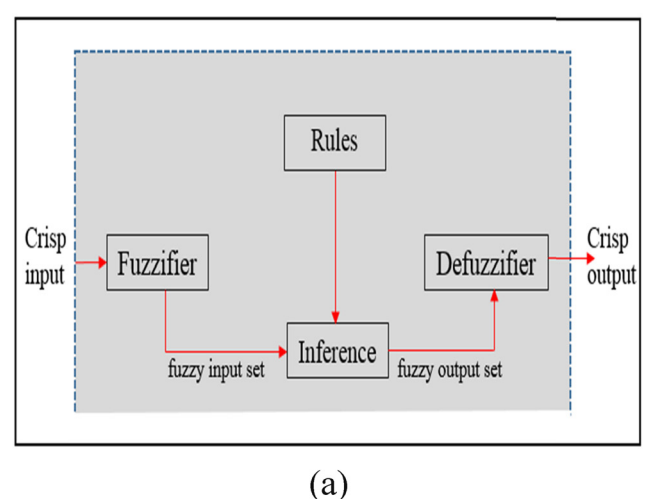
Notation H0	Sample temperature Ambient temperature (°C)	Notation	Wire feed rate
H ₁	100	S1	(Slow) = 2.5 m/min
H_2	150	S2	(Medium) = 5 m/min
H ₃	200	S3	(Fast) = 10 m/min

Table 3: Input welding parameters

Sample no.	Plate no.	Voltage (volt)	Current (amp)	Welding speed (mm/s)	Heat input (J/mm)
1	H0 S1	20.2	71	3.2	359
2	H0 S2	23	151	5.3	521
3	H0 S3	28	246	8.0	689
4	H1 S1	20.2	74	3.1	389
5	H1 S2	23	149	4.6	600
6	H1 S3	28.7	239	7.3	755
7	H2 S1	20	75	3.5	345
8	H2 S2	23	150	4.2	656
9	H2 S3	28.7	226	7.6	681
10	H3 S1	20.2	73	4.0	295
11	H3 S2	22.7	145	6.7	395
12	H3 S3	28.7	230	9.4	561

(20–25 V), moderate (22.5–27.5 V), and high (25–30 V) voltages; low (70–160 A), moderate (115–205 A), and high (160–250 A) currents; low (3–7 mm/s), moderate (5–9 mm/s), and high (7–11 mm/s) welding speeds as well as low (295–525 J), moderate (410–640 J), and high (525–755 J) heat inputs. These input variables were fuzzified by converting them into fuzzy sets, thereby normalizing

the data to prevent outliers. Fuzzification allows for the incorporation of uncertainty and imprecision inherent in the welding process, facilitating a more nuanced analysis. Linguistic terms were assigned to the fuzzy sets via fuzzy precursors (fuzzy interference, fuzzy reasoning, and fuzzy aggregation). This was followed by establishing Rule Base Commands (RBC) such as "IF-THEN" statements, which described the input-output parameter relationship. The RBC serves as the integral part of the FLA, dictating how inputs are translated into outputs. The FLA was developed by taking cognizance of the welding mathematical models, including transient heat transfer and fluid flow equations. Mamdani inference mechanism was adopted to derive fuzzy output sets from the fuzzy input sets. The inference mechanism is critical for synthesizing the information from the rule base, thereby producing accurate predictions. The next step in the modelling process was converting the fuzzy output response (weld bead geometric output parameters) into crisp data (Figure 6(a)) by selecting centroid as the defuzzification method. Defuzzification is essential for translating fuzzy outputs into actionable insights that can be utilized in welding practice. The last step in the FLA model architecture was to assess the accuracy and reliability of the model. Figure 6(b) represents information of the membership function designed for the fuzzification and defuzzification sequence,



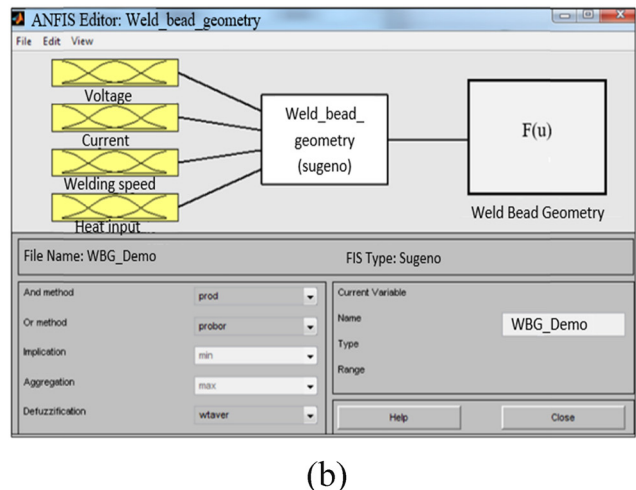


Figure 5: (a) Process diagram of fuzzy logic terms algorithm. (b) Defining input and output.

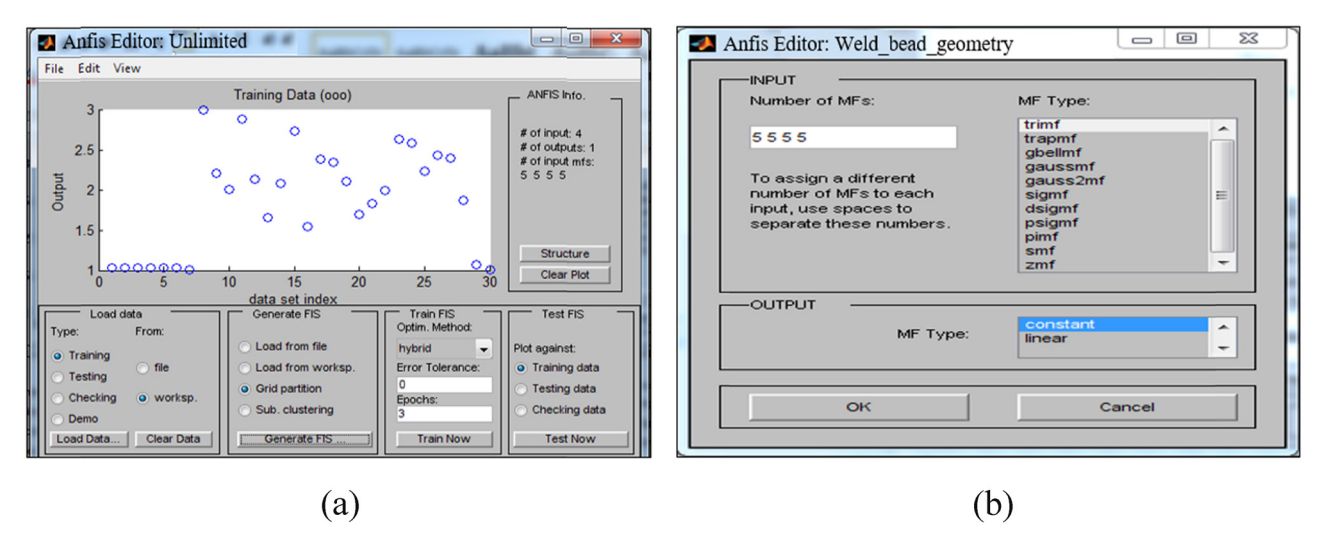


Figure 6: (a) ANFIS edit toolbox showing crisp data. (b) Description of input-output membership function.

as well as the process transformation of non-fuzzy input parameters to fuzzy linguistic terms. The construction of a fuzzy logic system model architecture for analysing the FCAW bead geometric characteristics of 1020 steel involves a systematic approach that encompasses the identification of input variables, data collection, fuzzification, rule-based development, inference, defuzzification, and model validation.

Membership function is an essential theory in the fuzzy logic modelling process in which a degree of membership is assigned by the fuzzy algorithm to an individual element in a fuzzy set. Applying this concept to the prediction of welding voltage, the welding input variable was considered as the voltage value, while output response was considered the degree of membership in the low, moderate, and high regime welding voltage fuzzy sets

(Figure 7(a) and (b)). In this case, the fuzzy set geometry is expounded by the membership function, which practically dictates the classification order of input values into one of the fuzzy sets. This information was also applied to welding current, welding speed, and heat input for predicting the weld bead width, height, depth of penetration, HAZ width, and HAZ height, respectively. Similarly, for the prediction of bead width, which in this case is one of the output responses considered in the present study, a membership function was employed for classifying the input variables identified earlier in this study into small, moderate, and wide geometries based on their linguistic terms, as shown in Figure 8(a) and (b). These linguistic terms are expounded based on the pattern of experimental values and expert knowledge in the FCAW welding sequence.

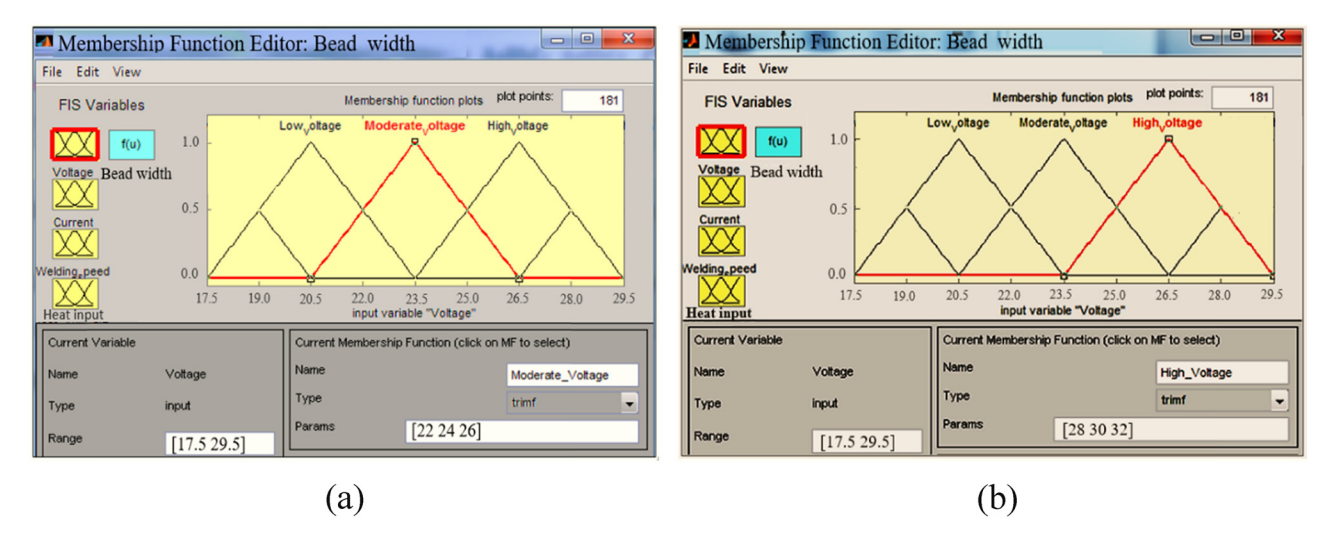


Figure 7: (a) Membership function for predicting moderate voltage input. (b) Membership function for predicting high voltage input.

8 — Abdulkareem Aloraier et al. DE GRUYTER

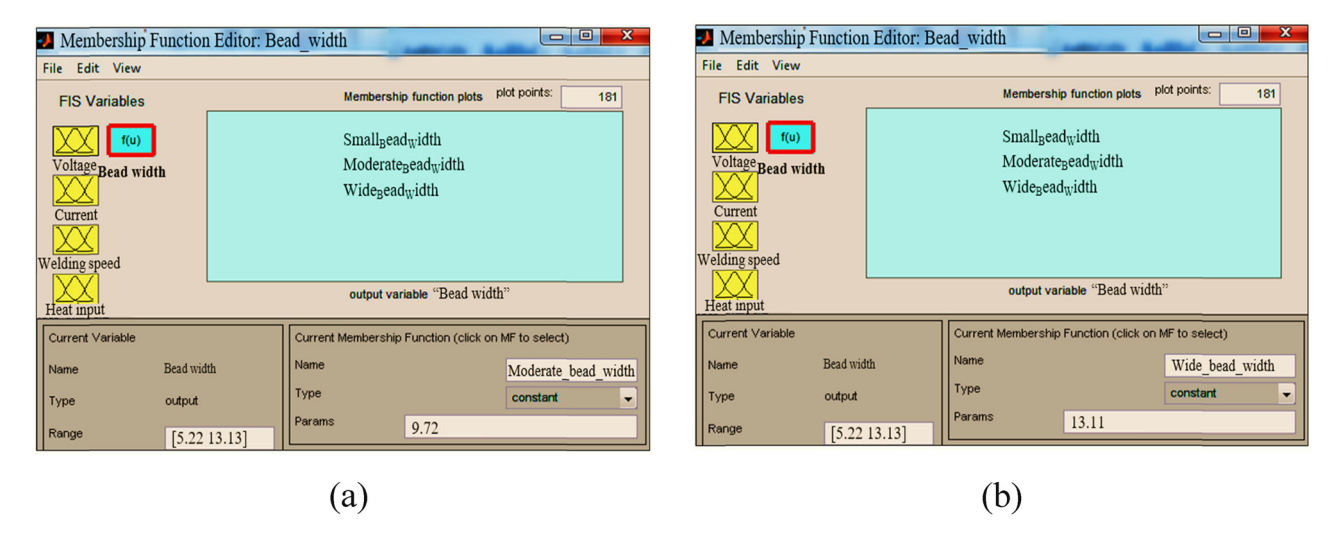


Figure 8: (a) Membership function for predicting moderate bead width. (b) Membership function for predicting wide bead width.

The information presented in this section was also applied to predict the bead width, height, depth of penetration, HAZ width, and HAZ height.

3 Results and discussion

The results obtained while analysing the combined effects of preheating and welding wire feed rates on the FCAW geometric bead characteristics of 1020 steel with integrated FLA for prediction of the weld bead geometry are presented and discussed in this section.

3.1 Micrographs of weld bead geometry

The integrity of a weld joint is dependent upon various factors, including the wire feed rate and heat input. Wire feed rate is a welding variable that relates to the flow rate at which the filler metal travels into the arc [21], whereas heat input is a welding variable that relates to the amount of energy that is transferred to the 1020 steel workpiece during the FCAW process [22,23]. In this study, wire feed rates of 2.5, 5, and 10 m/min and heat inputs of 347, 543, and 671 J/mm were considered during the FCAW process; each sample preheated at 100, 150, and 200°C prior to welding. Micrographs of the weld bead geometry are presented in Figure 9. Considering the effect of each variable (such as wire feed rate) intensities or values on the weld bead geometry in Figure 9, it can be observed that the combined effects of sample low preheating temperature of 100°C,

slow wire feed rate of 2.5 m/min, and low heat input of 347 J/mm resulted in a smaller weld pool and a narrow and shallow bead width. Similarly, the combined effects of the sample's medium preheating temperature of 150°C, wire feed rate of 5 m/min, and medium heat input of 543 J/mm were considered the moderate range for obtaining a balance between the integrity of welds and bead geometry. This is due to the slight increase in the size of the geometry, which was characterized by slight increment in the weld pool and bead width compared to the previous sample preheated at 100°C, as shown in Figure 9. Achieving moderate or optimal bead geometry from the FCAW process comes with several benefits, including improved mechanical properties, reduced distortion, and higher weld efficiency, leading to cost savings. However, combined effects of the 200°C sample preheated temperature, wire feed rate of 10 m/min, and heat input of 671 J/mm led to a larger weld pool, and a wide and deep weld bead, as shown in Figure 9. The implication of this findings lies on the fact that a narrow bead width may cause inadequate or shallow bead penetration, resulting in a frail weld joint [24], whereas a wide bead width has the tendency to cause distortion and intense heat input [25]. The geometry of a weld bead achieved via the FCAW process is a very sensitive factor due to its tendency to influence the weld strength and weld quality [26]. Therefore, the welding input parameters must be properly selected to prevent unwanted weld joint failure. Hence, it is essential to optimize these parameters to achieve the desired weld bead geometry and ensure the quality of the weld joint.

Welding parameters, depending on their intensities and interactions with one another, can influence the depth of bead penetration. Weld bead penetration, also referred to as "depth of fusion," is a welding component that relates

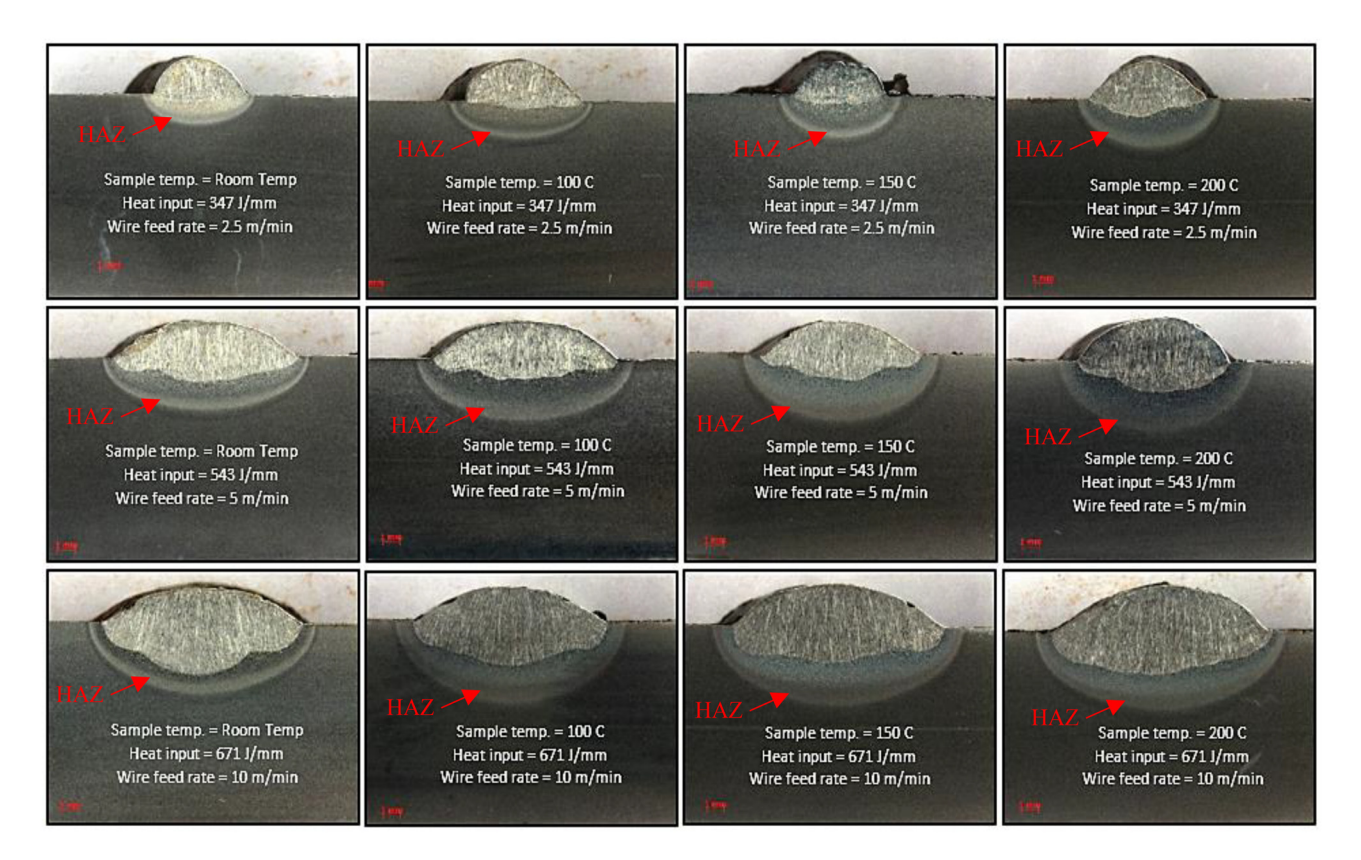


Figure 9: Macrographs of weld bead geometry for all samples.

to the distance extended by fusion into the base metal and also an essential parameter that dictates the weld strength [27]. The combined effects of the sample's low preheating temperature of 100°C, slow wire feed rate of 2.5 m/min, and low heat input of 347 J/mm achieved via the FCAW process resulted in a shallow penetration depth, as shown in Figure 9, which may cause insufficient fusion between the base material and the

Table 4: Experimental weld bead geometry and HAZ measurements (mm)

Sample No.	Bead width	Bead height	Depth of penetration	HAZ width	HAZ height
1	5.22	1.83	0.38	6.87	1.48
2	10.45	1.77	1.20	11.58	1.82
3	11.79	1.69	2.65	13.86	1.57
4	12.35	4.12	1.11	15.86	3.56
5	11.14	1.92	1.10	13.61	2.93
6	11.42	1.58	2.20	14.29	2.45
7	5.40	1.66	0.47	7.56	2.24
8	9.63	1.51	1.31	12.20	2.76
9	12.91	2.11	1.93	15.07	2.22
10	6.88	1.84	0.93	9.06	2.12
11	6.90	1.85	0.95	9.12	2.20
12	13.13	2.41	2.25	15.48	2.72

weld metal, poor mechanical properties as well as inadequate resistance to weld fatigue and cracking. However, the weld penetration depth was observed to increase slightly further with the medium preheating temperature of 150°C, wire feed rate of 5 m/min, and medium heat input of 543 J/mm. These parameters may be considered optimal for obtaining an ideal weld bead penetration. On the other hand, the combined effects of the 200°C sample preheated temperature, wire feed rate of 10 m/min, and heat input of 671 J/mm led to excessive penetration depth (Figure 9), which may induce distortion effects and base metal warping as well as undercut and burn-through defects. On the other hand, the application of the medium weld heat input is usually adjudged ideal for obtaining uniformity in depth of penetration and HAZ [28].

In this context, HAZ is a welding phenomenon that relates to the area of the base metal, which had been exposed to the effect of thermal cycles but had not undergone melting while conducting the FCAW welding process. The size and properties of the HAZ can be influenced by welding variables such as heat input, wire feed rate, preheat temperature etc. The combined effects of the sample's low preheating temperature of 100°C, slow wire feed rate of 2.5 m/min, and low heat input of 347 J/mm achieved via the FCAW process resulted in a smaller HAZ, as shown in Figure 9. These low welding parameters, which may not

Table 5: Summary of membership functions and sets for predicting weld bead geometry

Membership function	Membership set					
	Voltage	Current	Welding speed	Heat input		
Low	20, 22.5, 25	70, 115, 160	3, 5, 7	295, 410, 525		
Moderate	22.5, 25, 27.5	115, 160, 205	5, 7, 9	410, 525, 640		
High	25, 27.5, 30	160, 205, 250	7, 9, 11	525, 640, 755		

possess sufficient momentum or energy, partially affect the molecular or atomic structure of the material, causing low thermal distortion as well as minimal cracking effects on the welds [29,30]. However, it has a negative impact of insufficient bead penetration and lack of adequate fusion of the base metal, resulting in frail and low-quality welds. The bottom line may be balancing the low values of these parameters with other welding input variables to control the HAZ size and ensure good quality welds. On the other hand, while holistically considering the combined effects of these parameters, it is worth mentioning that each constituting parameters may have its individual effect on the weld. For example, the application of FCAW on a sample with low preheated temperature of 100°C may not provide adequate heat input to the base material to properly increase its temperature prior to welding [31]. Consequently, rapid cooling rate and solidification occurs on the welded metal, resulting in the formation of narrow HAZ. The implication of this is increased hardness and minimal toughness in the HAZ, which has the tendency of causing unwanted cracks [32,33]. Moreover, the low preheated sample temperature may not be effective enough for removal of moisture and associated impurities, thereby undermining the weld integrity.

The combined effects of the sample's medium preheating temperature of 150°C, wire feed rate of 5 m/min, and medium heat input of 543 J/mm were considered N ideal range of FCAW parameters that can produce an optimum HAZ size, as shown in Figure 9. These parameters provides optimum bead penetration while providing room for effective fusion between the weld joint, thereby producing long-lasting welds. Moreover, these parameters can conveniently manage the HAZ size by ensuring that excessive distortion and cracks are reduced to acceptable limits. Considering the effect of individual parameter, therefore, the medium sample preheated temperature of 150°C, a balance can still be obtained with the cooling and solidification rates, resulting in the formation of an optimal HAZ size. Consequently, adequate control of the FCAW process is achieved, allowing maximum fusion of the base material and filler metal. This provides significant benefit to the welds in terms of minimizing the effect of hydrogen cracking via the

removal of moisture content and impurities from the base metal. However, the application of high (about 200°C) or excessively high sample preheating temperature may result in excessive grain growth across the HAZ, compromising the mechanical properties of the welds [34]. Similarly, combined effects of the 200°C high sample preheated temperature, high wire feed rate of 10 m/min, and high heat input of 671 J/mm led to a larger HAZ size, as shown in Figure 9, compared to low and medium parametric ranges employed in this study. This can allow for the occurrence of excessive distortion on the welds, thereby intensifying the risk of hydrogen cracking, particularly in materials that are prone to thermal disintegration. Therefore, application of the aforementioned high FCAW parameters should be carefully controlled and optimized; by so doing, negative effects on the HAZ size and quality of welds can be minimized. However, when considering a sample preheating temperature of 200°C, the FCAW process may produce wider HAZ size as a result of the base metal being subjected to intense heating temperature [35]. This can prolong the cooling rate, increase the risk of cracking while accelerating the rate of grain growth, thermal distortion, and residual stresses due to elevated temperature (creep effect) and softening the HAZ. Consequently, welding conditions of this nature can trigger the burn-through effect, particularly when welding metals with low thickness. While also considering the effect of individual welding parameter, such as heat input, it is worth noting that the amount of arc energy supplied is not the only variable that affects the depth of penetration and HAZ formation, but also the dynamics between the welding process [36,37]. For example, during GTAW and GMAW processes, the control of the heat input is achieved by adjusting the welding current, voltage, and travel speed. Also, the heat input in SAW and FCAW is mainly determined by the welding current, voltage, speed, gas flow rate etc., while the flux and composition of the continuously fed filler metal can be used in controlling the heat input. The key features of the bead geometry experimentally obtained by the FCAW process are presented in Table 4. The data in Table 4 were experimentally obtained from the combined effects of the welding input variable, which interacted and reacted with each other to produce the output responses.

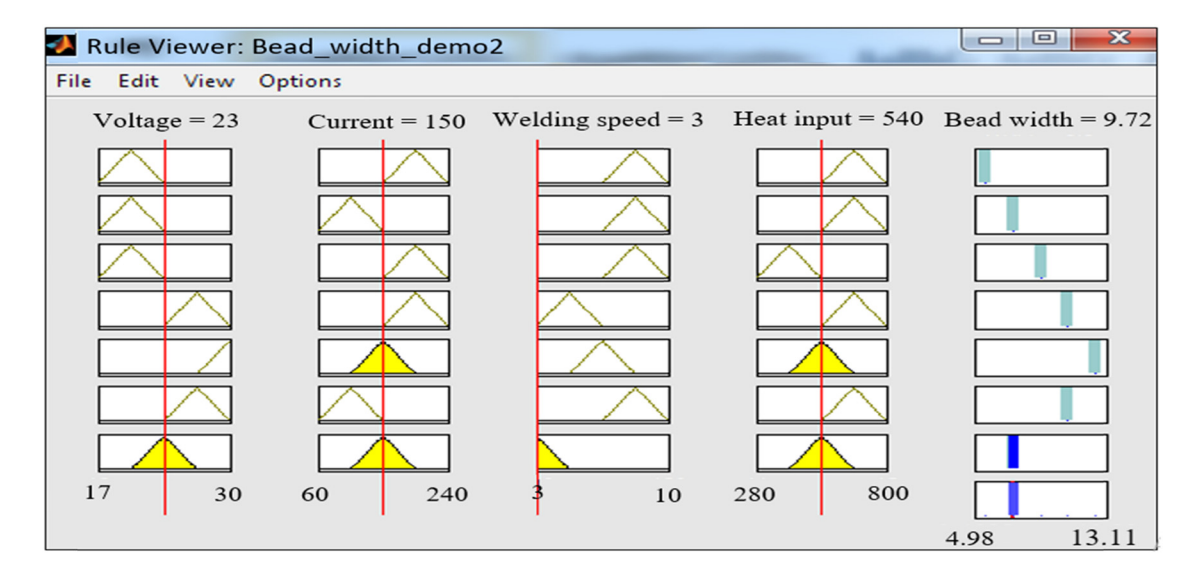


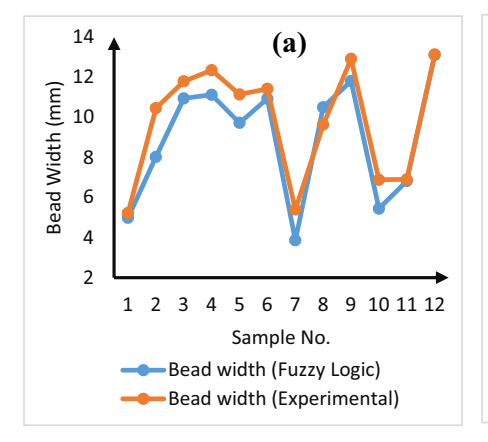
Figure 10: Fuzzy logic profile for predicting the optimal weld bead width.

3.2 Predicted bead geometry by using fuzzy logic

Membership functions and sets play a vital role in the prediction of weld bead geometry, as they serve as important tools for demystifying the complex and nonlinear relationships between welding input variables and the output response [38,39]. Appropriately specifying the fuzzy sets for input variables and defining ideal membership functions in this study aided the development of fuzzy-based expert models employed for predicting weld bead geometry based on the welding input variables. In this study, the fuzzy membership function and set for predicting weld bead geometry are summarized in Table 5.

The membership function was observed to possess a triangular shape, characterized by a peak at the lower end

of the voltage range on the fuzzy profile for predicting the low welding voltage. The shape is an indication that values closer to the lower end of the range had a higher degree of membership in the low voltage set. Moreover, the membership function can be observed with a triangular shape that is characterized by a peak at the middle of the voltage range on the profile for predicting moderate welding voltage (Figure 10). Similarly, in the case of low voltage, the shape is an indication that values around the middle of the range have a higher degree of membership in the moderate voltage set. On the other hand, the fuzzy profile for predicting the high welding voltage exhibited the membership function with a triangular shape characterized by a peak at the higher end of the voltage range, implying that values along the higher end of the range passed higher degree of membership in the high voltage set. The



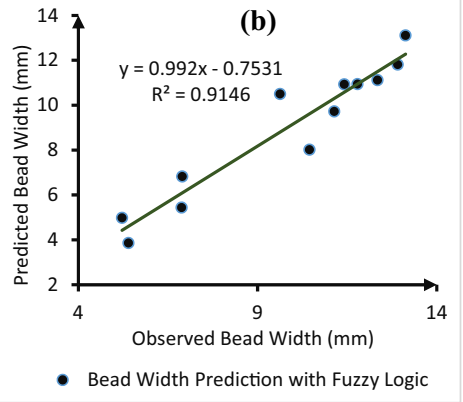
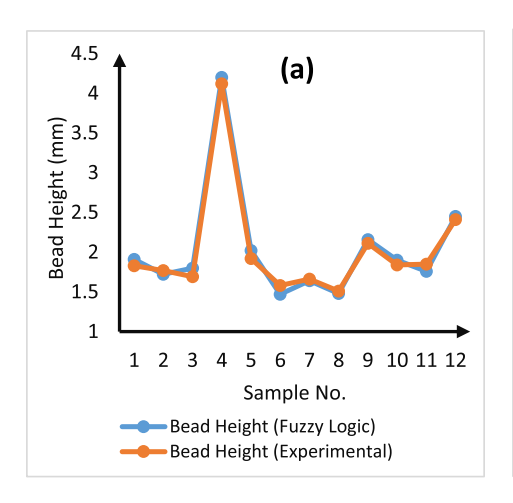


Figure 11: (a) Correlation plot for the fuzzy predicted and experimental bead width, and (b) regression plot for the fuzzy predicted and observed bead width.

12 — Abdulkareem Aloraier *et al.* DE GRUYTER



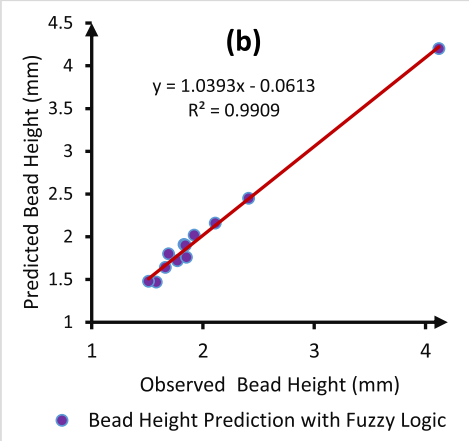
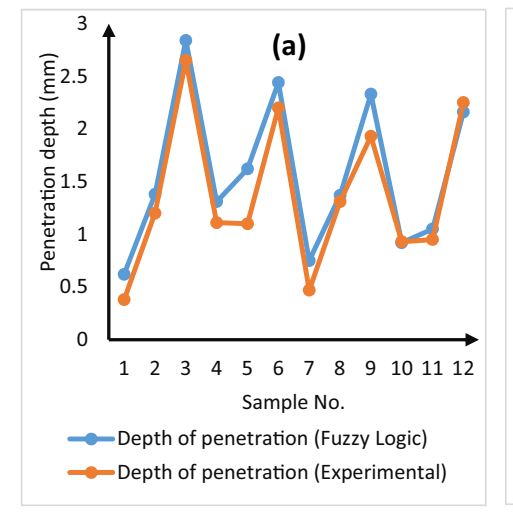


Figure 12: (a) Correlation plot for the fuzzy predicted and experimental bead height, and (b) regression plot for the fuzzy predicted and observed bead height.

information in this section also applied to the welding current, welding speed, and heat input. The fuzzy logic profile in Figure 10 indicates that a welding voltage of 23 V, a current of 150 A, a welding speed of 3 mm/s, and a heat input of 540 J/mm are the ideal input variables for predicting the optimal weld bead width of 9.72 mm, with the corresponding bead height, depth of penetration, HAZ width and HAZ height of 2.02, 1.62, 12.54 and 2.73 mm, respectively.

The correlation plot for the fuzzy predicted and experimental weld bead width, bead height, depth of penetration, HAZ width, and HAZ height are graphically presented in Figures 11(a), 12(a), 13(a), 14(a) and 15(a), respectively. On the other hand, the regression plot for the fuzzy predicted and observed weld bead width, bead height, depth of penetration, HAZ width, and HAZ height are graphically

presented in Figures 11(b), 12(b), 13(b), 14(b) and 15(b), respectively. Figure 11(a) demonstrates a strong correlation between the fuzzy predicted and experimental weld bead width, with the strongest correlation observed for sample No. 12. This further revealed the coefficient of determination R^2 value of 0.9146, as shown in Figure 11(b). Figure 12(a) demonstrates a significantly strong correlation between the fuzzy predicted and experimental weld bead height, with the strongest correlation observed for sample No. 7. This is further demonstrated in Figure 12(b), with an R^2 value of 0.9909. Figure 13(a) demonstrates a strong correlation between the fuzzy predicted and experimental depth of penetration, with the strongest correlation observed for sample No. 10. The correlation between these variables is greater than that of bead width, but less than that of the



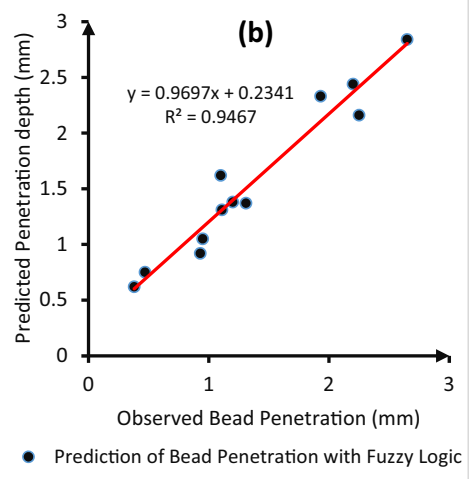
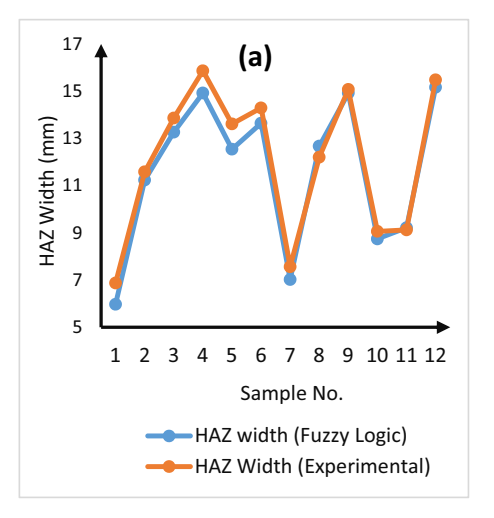


Figure 13: (a) Correlation plot for the fuzzy predicted and experimental depth of penetration, and (b) regression plot for the fuzzy predicted and observed depth of penetration.



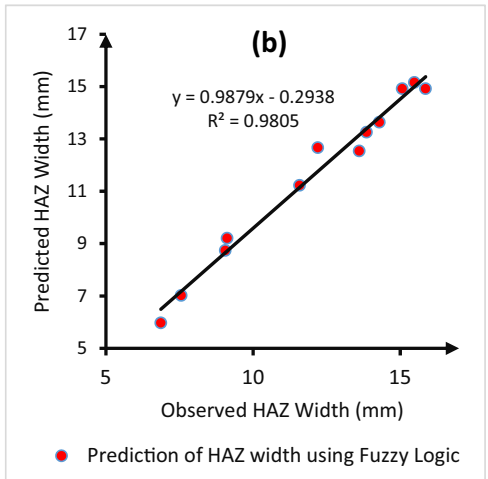
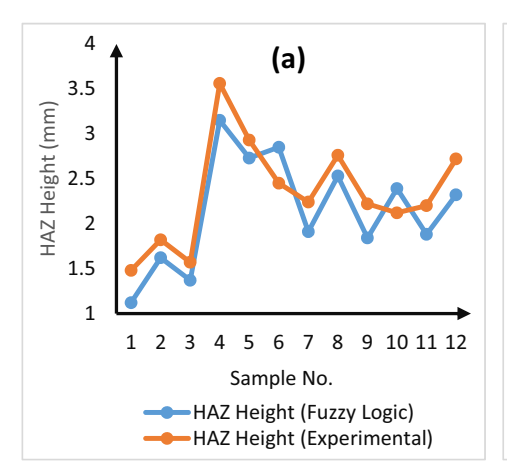


Figure 14: (a) Correlation plot for the fuzzy predicted and experimental HAZ width, and (b) regression plot for the fuzzy predicted and observed HAZ width.

bead height. This is further demonstrated in Figure 13(b), with a R^2 value of 0.9467. Figure 14(a) demonstrates a high degree of correlation between the fuzzy predicted and experimental HAZ width, which is close to that of bead height with the strongest correlation observed for sample No. 11. The correlation between these variables is obviously greater than that of bead width and depth of penetration. This is further demonstrated in Figure 14(b), with an R^2 value of 0.9805. Finally, Figure 15(a) demonstrates a mild degree of correlation between the fuzzy predicted and experimental HAZ height, which is less than that of the four [4] variables considered earlier, with the strongest correlation observed for samples No. 2, 3, and 5. This is further demonstrated in Figure 15(b), with an R^2 value of 0.8239. The application of advanced optimization algorithms, such as genetic algorithms or particle swarm optimization, can

facilitate the fine-tuning of model parameters, including the weights assigned to different input variables and the structure of the fuzzy inference system. These techniques can help identify optimal configurations that yield higher prediction accuracy for the HAZ height. Implementing a feedback loop, where model predictions are regularly compared with real-world outcomes can lead to parametric refinements and adjustments, resulting in a more accurate and reliable predictive model.

The regression plots, see Figures 11(b)–15(b), which typically consist of a scatter plot with the predicted values on the *y*-axis and the observed values on the *x*-axis, showed a visual illustration of the level of precision in which the predicted welding response was in agreement with the observed response. The accuracy of the fuzzy logic model in predicting the weld bead geometry, which is practically



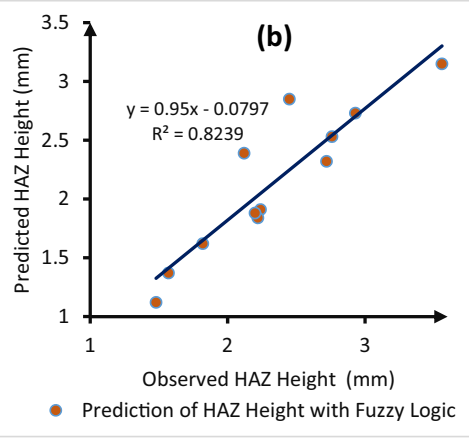


Figure 15: (a) Correlation plot for the fuzzy predicted and experimental HAZ height, and (b) regression plot for fuzzy predicted and observed HAZ height.

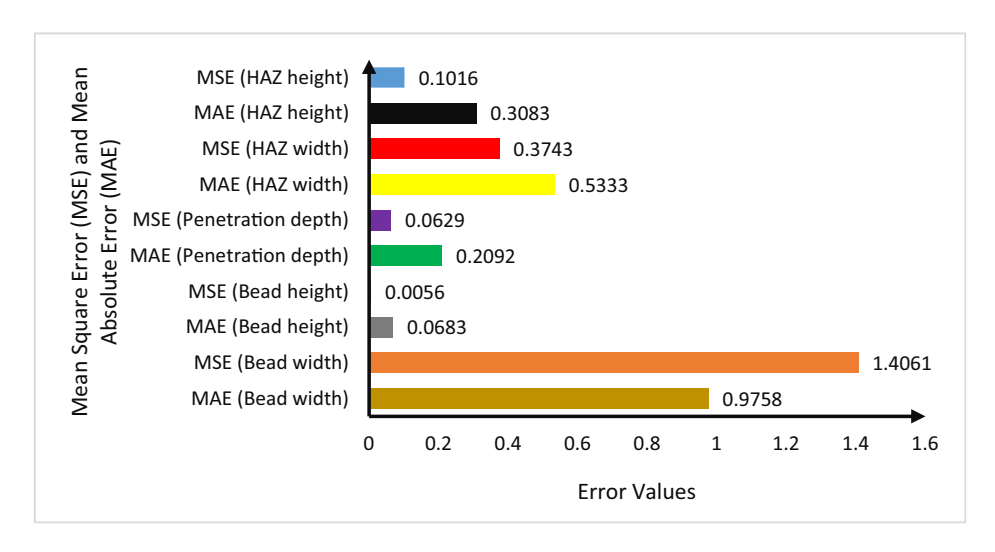


Figure 16: MSE and MAE metrics of the fuzzy models.

characterized by the bead width, bead height, depth of penetration, HAZ width, and height, was assessed *via* the regression plot. This provided a clue about the discrepancies between the predicted and observed values. The plot also included a regression line that represents the best-fit line with the data points. The closer the data points are to the regression line, the better the model is at predicting the observed values [40]. The plot was analysed by examining the distribution of data points around the regression line.

Figure 16 shows the mean square error (MSE) and mean absolute error (MAE) metrics of fuzzy logic weld bead geometric models in this study, including the bead width, bead height, penetration depth, HAZ width, and HAZ height. The MSE and MAE values obtained for all of the output parameters on the fuzzy models are below 0.55, whereas the error values obtained for the bead width are higher, specifically 0.9758 and 1.4061. This implies that fuzzy logic models employed in this analysis are reliable for the predicting FCAW output welding response. Although the computed errors for the bead width geometry slightly increased compared to the other error values, by implementation of some optimization techniques, such as feature selection, hyper-parameter tuning, model complexity adjustment and integration of ensemble methods, the error metrics can be minimized.

4 Conclusion

The microstructures of FCAW weld bead geometries examined in this study included the fusion zone, HAZ, and the base metal, which are crucial in determining the weld

mechanical properties, such as ductility, strength, hardness, toughness etc. From the findings of this study, the welding input variables such as voltage, current, welding speed, and heat input can positively or negatively influence the weld microstructure as well as its mechanical properties. For example, the study revealed that a finegrained microstructure in the fusion zone is desirable for achieving high strength and toughness, while a coarsegrained microstructure in the heat-affected zone may lead to reduced mechanical properties. The microstructural study revealed that the heat input and depth of penetration are the key parameters that are influenced by the FCAW process voltage. This is because the application of a higher welding voltage works with longer arc length, which increases the rate of heat input while deepening the depth of penetration. Welding voltage when applied excessively can cause spatters around the fusion zone and poor bead geometry. However, the study further revealed that the heat input and bead width are the common parameters influenced by the FCAW process current. This is because the application of higher welding current is accompanied by a higher deposition rate, which increases the heat input while widening the bead width, thereby resulting in distortion and poor weld fusion when applied excessively. On the other hand, the cooling rate, bead shape, and width of fusion zone were observed as the primary components affected by the welding speed of the FCAW process. This is because the application of the higher FCAW process speed is one of the welding mechanisms that causes faster cooling rate, thereby producing the flatter bead shape and narrow width of the fusion zone. Welding speed when used excessively can lead to incomplete fusion and lack of penetration. Finally, the size of the

HAZ, macrostructures, and microstructures were observed to be influenced by the heat input of the FCAW process, as larger HAZ and coarser microstructure are induced by the higher heat input. However, its excessive application may cause distortion and cracking of the weld. Therefore, it is crucial to control and optimize these welding variables in order to achieve the desired microstructural bead geometry for 1020 steel.

A strong correlation was observed between the predicted and experimental values, signifying the robustness of the fuzzy logic model in demystifying the complex relationships between input variables and the weld bead width, which directly affects the strength and integrity of the joint. Bead height is another important parameter that influences the mechanical properties of the weld. A significantly high degree of correlation was noted between the predicted and experimental values of the bead height (which directly influences the weld mechanical properties), signifying that the fuzzy logic model effectively identified the variations associated with the bead height with a high level of accuracy. This is similar to the HAZ width (an essential indicator of the thermal effects of welding on the base metal), which also demonstrated a very strong correlation between the predicted and experimental values. In addition, a significant agreement was established between the predicted and experimental values of the depth of penetration, signifying the reliability of the fuzzy logic model in the prediction of depth of penetration. For the HAZ height, the correlation though not too strong did not indicate a significant deviation between the predicted and experimental values. A tight cluster of data points was observed around the regression lines (Figures 11(b)-15(b)), signifying a high degree of correlation between the predicted and observed values, suggesting that the fuzzy logic model is accurate in predicting the weld bead geometry.

Acknowledgments: The authors would like to acknowledge the support and help provided by Dr. Abdullah Al-Hindal and Engineer Mohammad Rajab from the Nanoscopic Center, Faculty of Science, Kuwait University, Kuwait.

Funding information: Authors state no funding involved.

Author contributions: All authors contributed to the study conception and design. Material preparation, data collection, and analysis were performed by all authors. All authors have accepted responsibility for the entire content of this manuscript and approved its submission.

Conflict of interest: Authors state no conflict of interest.

Data availability statement: All data generated or analysed during this study are included in this published article.

References

- Kumar A, Sundarrajan S. Optimization of pulsed TIG welding process parameters on mechanical properties of AA 5456 Aluminum alloy weldments. Mater Des. 2009;30(4):1288–97.
- [2] Thao D, Kim I. Interaction model for predicting bead geometry for Lab Joint in GMA welding process. Comput Mater Sci Surf Eng. 2009:1(4):237–44.
- [3] Dhas J, Kumanan S. ANFIS for prediction of weld bead width in a submerged arc welding process. J Sci Ind Res. 2007;66:335–8.
- [4] Kumar V. Modeling of weld bead geometry and shape relationships in submerged arc welding using developed fluxes. Jordan J Mech Ind Eng. 2011;5:461–70.
- [5] Gautam U, Abbas M. Analysis of weld bead geometry in saw and modeling using CCD. Int J Mech Eng Robot Res. 2013;2(3):168–81.
- [6] Balasubramanian K, Vikram R, Sambath S, Sowrirajan M, Arunachalashiva M, Abhijith P, et al. Optimization of flux cored arc welding parameters to minimize the dilution percentage of AISI 316L stainless steel cladding on mild steel. Int J Interact Des Manuf. 2025;19(1):55–65.
- [7] Moreno JRS, Guimarães JB, da Silva Lizzi EA, Correa CA. Analyze and optimize the welding parameters of the process by pulsed tubular wire (FCAW-flux cored arc welding) based on the geometry of the weld beads resulting from each test. J Mater Sci Technol Res. 2022;9(1):11–23.
- [8] Moreno J, Pinto H, Ávila J. Characterization of welding parameters and microstructure in a coating made with a tubular electrode of SAE EC410NiMo on a SAE 1020 steel substrate by FCAW process. Conference: 21st International Conference Materials, Methods & Technologies; 2019.
- [9] Abhishek K, Prajapati V, Kumari S, Potnuru BK, Bandhu D. Application of metal cored filler wire for environmental-friendly welding of low alloy steel: experimental investigation and parametric optimization. Int J Interact Des Manuf. 2024;18(10):7445–58.
- [10] Tomaz IDV, Colaço FHG, Sarfraz S, Pimenov DY, Gupta MK, Pintaude G. Investigations on quality characteristics in gas tungsten arc welding process using artificial neural network integrated with genetic algorithm. Int J Adv Manuf Technol. 2021;113(11):3569–83.
- [11] Colaço FHG, Pintaude G. Combined effects on Fe-Cr-C hardfacing deposited by new technique FCDW-GTAW. Matéria. 2022;26:e13097.
- [12] Acharya S, Patra S, Das S. Predicting A-TIG weld bead geometry of 304 stainless steel using artificial neural networks. Discover Mech Eng. 2025;4(1):12.
- [13] Yang G, Liu X, Lai J, Wei Y. Fatigue life prediction of gasoline storage tank considering varying current density and weld stress. Adv Mech Eng. 2022;14(6):16878132221104307.
- [14] Bagheri M, Zhu S-P, Ben Seghier MEA, Keshtegar B, Trung N-T. Hybrid intelligent method for fuzzy reliability analysis of corroded X100 steel pipelines. Eng Comput. 2021;37:2559–73.
- [15] Liang Z, Liu X, Yansong W, Wang X. Universal grey number theory for the uncertainty presence of wiper structural system. Assem Autom. 2021;41(1):55–70.

- [16] Yang S, Meng D, Wang H, Yang C. A novel learning function for adaptive surrogate-model-based reliability evaluation. Philos Trans R Soc A. 2024;382(2264):20220395.
- [17] Yang S, Meng D, Wang H, Chen Z, Xu B. A comparative study for adaptive surrogate-model-based reliability evaluation method of automobile components. Int J Struct Integr. 2023;14(3):498–519.
- [18] Meng D, Li Y, He C, Guo J, Lv Z, Wu P. Multidisciplinary design for structural integrity using a collaborative optimization method based on adaptive surrogate modelling. Mater Des. 2021;206:109789.
- [19] Liu X, Ma M. Cumulative fatigue damage theories for metals: review and prospects. Int J Struct Integr. 2023;14(5):629–62.
- [20] Springer Nature SingaporeIkpe A, Ndon A-I, Etim P. Fuzzy modelling and optimization of anaerobic co-digestion process parameters for effective biogas yield from bio-wastes. Int J Energy Eng Sci. 2020;5(2):43–61.
- [21] Thakar HH, Chaudhari MD, Vora JJ, Patel V, Das S, Bandhu D, et al. Performance optimization and investigation of metal-cored filler wires for high-strength steel during gas metal arc welding. High Temp Mater Process. 2023;42(1):20220305.
- [22] Bassey MO, Ohwoekevwo JU, Ikpe AE. Thermal analysis of AISI 1020 low carbon steel plate agglutinated by gas tungsten arc welding technique: a computational study of weld dilution using finite element method. J Eng Appl Sci. 2024;71(1):33.
- [23] Tarmizi T, Hananda NA, Irfan I. The effect of heat input on welding combination of GTAW and SMAW SA537 material on mechanical properties and microstructure. Kapal. 2022;19(2):56–63.
- [24] Ikpe A, Owunna I. Effects of parametric variations on bead width of gas tungsten arc welding of AISI 1020 low carbon steel plate. Int J Eng Technol Sci. 2018;5(3):1–13.
- [25] Owunna I, Ikpe A, Achebo J. 3D finite element modelling of weld bead penetration in tungsten inert gas (TIG) welding of AISI 1020 low carbon steel plate. Eur Mech Sci. 2018;2(3):96–105.
- [26] Benyounis K, Olabi A-G. Optimization of different welding processes using statistical and numerical approaches—A reference guide. Adv Eng Software. 2008;39(6):483–96.
- [27] Wang Z, Li L, Chen H, Wu X, Dong Y, Tian J, et al. Penetration recognition based on machine learning in arc welding: a review. Int I Adv Manuf Technol. 2023;125(9):3899–923.
- [28] Mehdi H, Mishra R. Consequence of reinforced SiC particles on microstructural and mechanical properties of AA6061 surface

- composites by multi-pass FSP. J Adhes Sci Technol. 2022;36(12):1279–98.
- [29] Yongbing L. Pressure welding. The ECPH encyclopedia of mining and metallurgy. Singapore: Springer Nature Singapore; 2024. p. 1685–6.
- [30] Lin C-M, Lu C-H. Effects of tempering temperature on microstructural evolution and mechanical properties of high-strength low-alloy D6AC plasma arc welds. Mater Sci Eng A. 2016;676:28–37.
- [31] Tang J, Shen Y. Effects of preheating treatment on temperature distribution and material flow of aluminum alloy and steel friction stir welds. | Manuf Process. 2017;29:29–40.
- [32] Mei Y, Liu Y, Liu C, Li C, Yu L, Guo Q, et al. Effect of base metal and welding speed on fusion zone microstructure and HAZ hot-cracking of electron-beam welded Inconel 718. Mater Des. 2016;89:964–77.
- [33] Banerjee K. Improving weldability of an advanced high strength steel by design of base metal microstructure. J Mater Process Technol. 2016;229:596–608.
- [34] Khan MS, Soleimani M, Midawi AR, Aderibigbe I, Zhou YN, Biro E. A review on heat affected zone softening of dual-phase steels during laser welding. J Manuf Process. 2023;102:663–84.
- [35] Choi D, Lee H, Cho S-K, Kim HC, Hyun S-K, Shin SY. Microstructure and charpy impact properties of FCAW and SAW heat affected zones of 100 mm thick steel plate for offshore platforms. Met Mater Int. 2020;26:867–81.
- [36] Mezaache M, Benaouda OF, Kellai A. Maximizing welding efficiency: applying an improved whale optimization algorithm for parametric optimization of bead width in a submerged arc welding process. Int | Adv Manuf Technol. 2024;134(5):2737–52.
- [37] Shravan C, Radhika N, Deepak Kumar NH, SivaSailam B. A review on welding techniques: properties, characterisations and engineering applications. Adv Mater Process Technol. 2023;10:80.
- [38] Gyasi EA, Handroos H, Kah P. Survey on artificial intelligence (AI) applied in welding: A future scenario of the influence of AI on technological, economic, educational and social changes. Procedia Manuf. 2019;38:702–14.
- [39] Khanzadeh M, Chowdhury S, Marufuzzaman M, Tschopp MA, Bian L. Porosity prediction: Supervised-learning of thermal history for direct laser deposition. J Manuf Syst. 2018;47:69–82.
- [40] Gauch HG, Hwang JG, Fick GW. Model evaluation by comparison of model-based predictions and measured values. Agron J. 2003;95(6):1442–6.